universe

IMPACT FACTOR 2.5

CITESCORE 4.3

Article

New Results of the Experiment to Search for Double Beta Decay of ^{106}Cd with Enriched $^{106}CdWO_4$ Scintillator

P. Belli, R. Bernabei, F. Cappella, V. Caracciolo, R. Cerulli, F. A. Danevich, A. Incicchitti, D. V. Kasperovych, V. R. Klavdiienko, V. V. Kobychev et al.

Special Issue

Exploring Double Beta Decay: Probing Fundamental Properties of Neutrinos and Beyond

Edited by

Prof. Dr. Rita Bernabei

MDPI

https://doi.org/10.3390/universe11040123

universe

MDPI

Article

New Results of the Experiment to Search for Double Beta Decay of ^{106}Cd with Enriched $^{106}CdWO_4$ Scintillator

P. Belli [1,2], R. Bernabei [1,2], F. Cappella [3,4], V. Caracciolo [1,2], R. Cerulli [1,2], F. A. Danevich [1,5], A. Incicchitti [3,4], D. V. Kasperovych [5], V. R. Klavdiienko [5], V. V. Kobychev [5], A. Leoncini [1,2], V. Merlo [1,2], O. G. Polischuk [5] and V. I. Tretyak [5,6,*]

1 INFN Sezione Roma "Tor Vergata", I-00133 Rome, Italy; pierluigi.belli@roma2.infn.it (P.B.); rita.bernabei@roma2.infn.it (R.B.); vincenzo.caracciolo@roma2.infn.it (V.C.); riccardo.cerulli@roma2.infn.it (R.C.); danevich@lngs.infn.it (F.A.D.); alice.leoncini@roma2.infn.it (A.L.); vittorio.merlo@roma2.infn.it (V.M.)
2 Dipartimento di Fisica, Università di Roma "Tor Vergata", I-00133 Rome, Italy
3 INFN Sezione Roma, I-00185 Rome, Italy; fabio.cappella@roma1.infn.it (F.C.); antonella.incicchitti@roma1.infn.it (A.I.)
4 Dipartimento di Fisica, Università di Roma "La Sapienza", I-00185 Rome, Italy
5 Institute for Nuclear Research of NASU, 03028 Kyiv, Ukraine; dkasper@kinr.kiev.ua (D.V.K.); klavdiienko.volodymyr@kinr.kiev.ua (V.R.K.); kobychev@kinr.kiev.ua (V.V.K.); polischuk@kinr.kiev.ua (O.G.P.)
6 Laboratori Nazionali del Gran Sasso, INFN, I-67100 Assergi, Italy
* Correspondence: vladimir.tretyak@lngs.infn.it

Abstract: In this article, we present current results of the experiment searching for double beta decay of ^{106}Cd with the help of an enriched $^{106}CdWO_4$ crystal scintillator in coincidence with two $CdWO_4$ scintillation detectors. The experiment is carried out at the Gran Sasso underground laboratory of the National Institute for Nuclear Physics (LNGS INFN, Italy). After 1075 days of data-taking, no double-beta effects were observed. New half-life limits have been set for the different modes and channels of double beta processes in ^{106}Cd at the level of lim $T_{1/2} = 10^{20} - 10^{22}$ years.

Keywords: double beta decay; 106Cd; 106CdWO4; crystal scintillator; low background measurements

check for updates

Academic Editor: Máté Csanád

Received: 13 February 2025
Revised: 25 March 2025
Accepted: 25 March 2025
Published: 7 April 2025

Citation: Belli, P.; Bernabei, R.; Cappella, F.; Caracciolo, V.; Cerulli, R.; Danevich, F.A.; Incicchitti, A.; Kasperovych, D.V.; Klavdiienko, V.R.; Kobychev, V.V.; et al. New Results of the Experiment to Search for Double Beta Decay of ^{106}Cd with Enriched $^{106}CdWO_4$ Scintillator. *Universe* **2025**, *11*, 123. https://doi.org/10.3390/universe11040123

Copyright: © 2025 by the authors. Licensee MDPI, Basel, Switzerland. This article is an open access article distributed under the terms and conditions of the Creative Commons Attribution (CC BY) license (https://creativecommons.org/licenses/by/4.0/).

1. Introduction

Despite the great success of the Standard Model of particles and interactions (SM), neutrino remains the least studied particle due to its extremely weak interaction with matter. In addition, experimentally observed left-handed neutrino states are massless particles according to SM. On the other hand, the observation of the neutrino oscillation provides insight into a non-zero mass of at least two of the three neutrino states [1]. Unfortunately, neutrino oscillation experiments do not give the absolute values of the neutrino masses and the neutrino mass hierarchy [2]. It is also an open question whether neutrinos are of Dirac or Majorana nature. The existence of massive Majorana neutrinos causes the violation of the lepton number symmetry [3–6] that could explain an asymmetry between matter and antimatter in the Universe [7]. One of the most promising approaches to elaborate the properties of neutrino is the study of the neutrinoless mode of double beta decay ($0\nu2\beta$) of atomic nuclei [8–13].

Double beta decay is the rarest nuclear process, with half-lives of $T_{1/2} = 10^{18}$–10^{24} years [14,15]. The process, comprising a nuclear charge increase by

two units and the emission of two electron and antineutrino pairs ($2\nu2\beta^-$), has been detected in 11 nuclei (^{48}Ca, ^{76}Ge, ^{82}Se, ^{96}Zr, ^{100}Mo, ^{116}Cd, ^{128}Te, ^{130}Te, ^{136}Xe, ^{150}Nd, and ^{238}U). There are also possible "double beta plus" processes characterized by a decrease in nuclear charge by two units: double electron capture (2EC), electron capture with positron emission (ECβ^+), and double positron decay ($2\beta^+$). The experimental sensitivity to the double beta plus processes is substantially lower. There are three indications of 2ν2EC decay: ^{78}Kr (in experiment with a proportional counter [16]), ^{130}Ba (in two geochemical experiments [17,18]), and ^{124}Xe [19–21]. The $2\nu2\beta$ decay, allowed in the SM, does not depend on the nature of the neutrino and the absolute neutrino mass scale, though it is very useful for testing theoretical approaches to describe 2β processes [9].

The most sensitive experiments searching for $0\nu2\beta$ decay reach half-life sensitivity at the level of $T_{1/2} > (0.05 - 3.8) \times 10^{26}$ years, which corresponds to the Majorana neutrino mass limits in the range $m_\nu < (0.03 - 0.6)$ eV [22–27]. These and future more sensitive experiments focus on the search for $0\nu2\beta^-$ decay. However, the physical mechanisms that violate lepton number symmetry in "double beta plus" processes are essentially the same as for the decay with electrons emission. 0νECβ^+ and $0\nu2\beta^+$ decays study is also motivated by the opportunity to clarify the possible contribution of the right-handed currents to the $0\nu2\beta^-$ decay [28]. In addition, resonant enhancement is possible in the $0\nu2EC$ process that could cause an increase in the transition probability by up to six orders of magnitude [29–32].

The ^{106}Cd nuclide is a promising candidate to search for double beta plus decays, thanks to several features. This nuclide has one of the highest transition energies $Q_{2\beta} = 2775.39(10)$ keV [33] and a comparatively high isotopic abundance $\delta = 1.245(22)\%$ [34]. A simplified decay scheme of ^{106}Cd is presented in Figure 1. There is also the availability of enrichment methods using gas centrifugation to consider. A crucial point is that there are well developed methods of cadmium purification and the existence of technology to produce high-quality radiopure cadmium tungstate ($CdWO_4$) crystal scintillators [35,36] that can be used in calorimetric experiments with a high detection efficiency. This approach was implemented in the present experiment, searching for the 2β decay of ^{106}Cd.

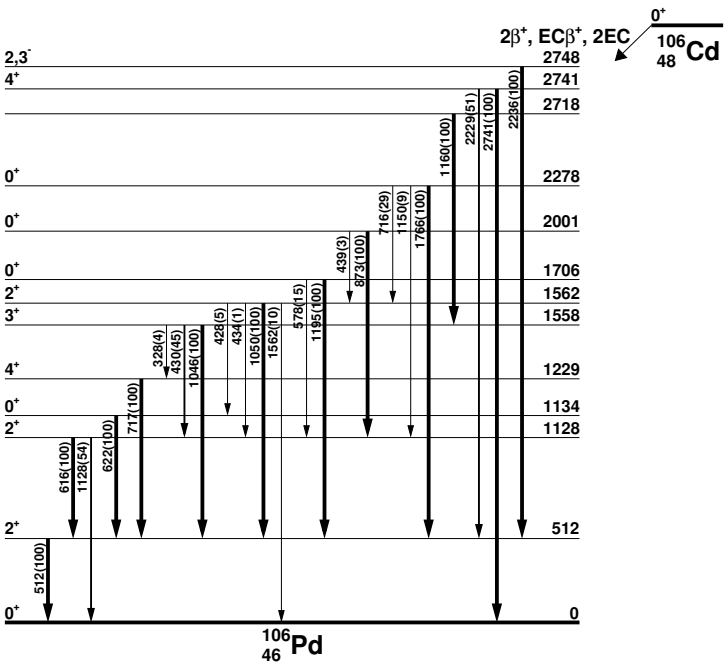

Figure 1. A simplified 2β decay scheme of ^{106}Cd. Energies of the γ-rays and excited levels of ^{106}Pd are given in keV. Levels from 2283 keV to 2714 keV and above 2748 keV are omitted. The thickness of the arrow is proportional to the gamma quanta relative emission intensity.

2. Experimental Setup

A schematic diagram of the experimental setup is shown in Figure 2. The main part of the detector system is three $CdWO_4$ crystal scintillators. A central near-cylindrical-shaped scintillator with dimensions ⌀27 mm × 50 mm and mass 215.4 g is enriched with ^{106}Cd to 66% ($^{106}CdWO_4$) [36]. The scintillator is viewed by low radioactive photomultiplier tube (PMT) Hamamatsu R11065-MOD through a high-purity quartz light-guide (⌀66 mm × 100 mm) and polystyrene-based plastic scintillator (⌀40 mm × 83 mm). A Teflon spring is installed between the crystal scintillator and the copper brick to ensure the optical contact between the $^{106}CdWO_4$ detector components. Two high volume $CdWO_4$ scintillators (⌀70 mm × 38 mm; with the natural cadmium abundance) have cylindrical cutouts to tightly enclose the $^{106}CdWO_4$ crystal. The $CdWO_4$ scintillators are viewed by radiopure PMTs Hamamatsu R6233MOD through high-purity quartz light-guides (⌀70 mm × 200 mm). Optical contacts between the detector details are treated with optical-grade silicone grease. To improve the light collection, the detector system is wrapped in Teflon tape and aluminized plastic film. The Teflon holds all the components together to ensure the detector system's geometry. To reduce background interference from PMTs, the detectors are surrounded by high-purity copper bricks ("internal copper"). The detector system is placed in a 11 cm-thick high-purity copper box ("external copper") surrounded by low-radioactive lead (15 cm), cadmium (2 mm), and polyethylene (10 cm). The inner volume of the copper box is continuously flushed with high-purity N_2 gas with a low radon contamination (<58 mBq/m^3 [37]) to remove radon present in environmental air. The experiment is carried out at 3.8 km of water equivalent depth at the Gran Sasso underground laboratory of the National Institute for Nuclear Physics (LNGS INFN, Italy).

The event-by-event data acquisition system is realized using a 1-GSample/s 8-bit transient digitizer DC270 by Agilent Technologies with a bandwidth of 250 MHz. The system records the shape of each signal in 100 μs time window with a 50 ns time bin. The $CdWO_4$ scintillator has a relatively long decay time with four components: ∼15 μs (89%); ∼4.6 μs (9%); ∼0.8 μs (2%); and ∼0.15 μs (0.5%) [38]. The first 100 time bins (5 μs) are used to calculate the mean value of the baseline. The energy of the event in the scintillator (E) is evaluated as the area of the digitized waveform:

$$E = \sum f(t_k), \quad (1)$$

where the sum is over time channels k, starting from the origin of the signal up to 25 μs, and $f(t_k)$ is the digitized waveform (at the time t_k) of a given signal after subtraction of the mean value of the baseline.

To reduce the data volume caused by β decays of ^{113}Cd (Q_β = 324 keV) and ^{113m}Cd (Q_β = 587 keV) nuclides, present in the $^{106}CdWO_4$ crystal [36,39], the data acquisition system recorded events when one of two conditions was met:

(1) an event in the $^{106}CdWO_4$ detector with an energy > 0.5 MeV;
(2) an event in the $^{106}CdWO_4$ detector with an energy > 0.05 MeV in coincidence with a signal in at least one of the $CdWO_4$ counters with energy > 0.05 MeV.

Despite a high counting rate (∼15 Hz) below ∼0.6 MeV, the presence of ^{113m}Cd nuclide in the $^{106}CdWO_4$ scintillator made it possible to monitor the stability of the detector system by analyzing the position of its β spectrum edge. More information about the $^{106}CdWO_4$ and $CdWO_4$ detectors stability can be found in [40]. The main reason for the energy scale time shift of the $^{106}CdWO_4$ detector was the degradation of the PMTs gain. Therefore, after 649 days of data taking, the PMT of the $^{106}CdWO_4$ detector was replaced with another unit of the same model. Additionally, a Teflon pipe was installed, which made it possible

to periodically calibrate the detector system with γ sources without switching off the high voltage and opening the setup.

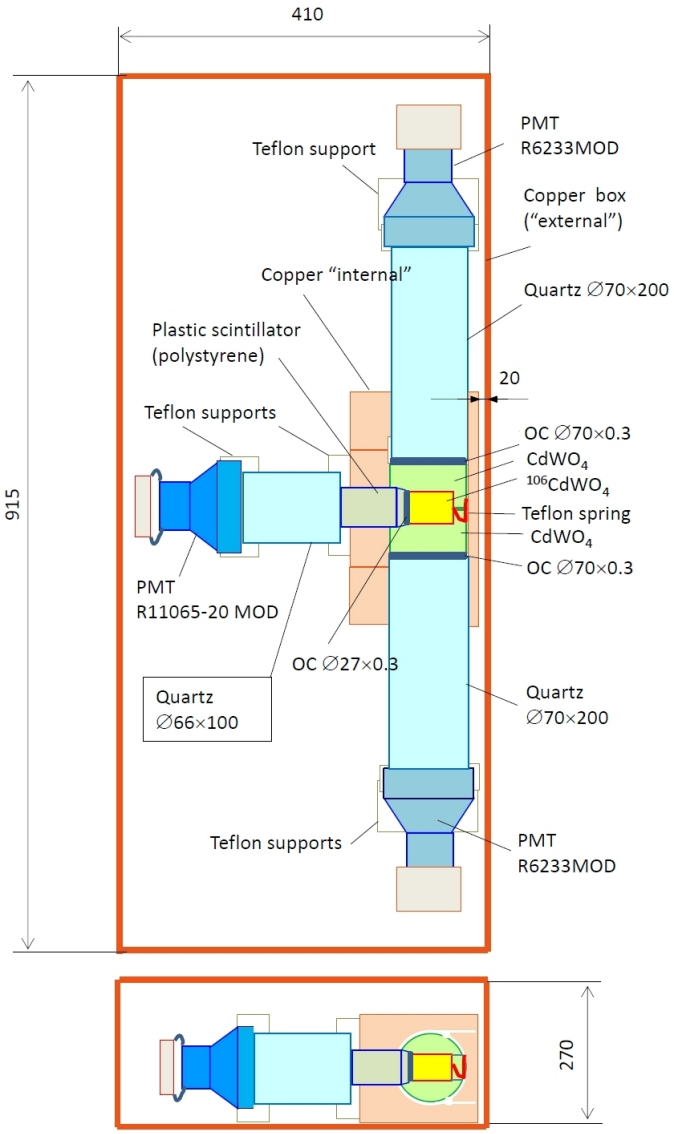

Figure 2. Schematic of the experimental set-up with the $^{106}CdWO_4$ scintillation detector. PMT denotes photomultiplier tube. OC refers to optical couplant. Dimensions are given in mm.

3. Data Analysis

3.1. Energy and Time Resolutions

The detector system was calibrated using ^{22}Na, ^{60}Co, ^{137}Cs, and ^{228}Th γ-ray sources in the beginning, and several times during the experiment. The energy spectra of the sources measured by the $^{106}CdWO_4$ and one of the $CdWO_4$ detectors are shown in Figure 3. The energy resolution of the detectors can be described by the function FWHM = $A \times \sqrt{E_\gamma}$, where E_γ is the energy of γ-ray quanta in keV, FWHM is the full width at half maximum in keV, and A is a constant. For the entire data set, the averaged value of A is equal to 4.92 for the $^{106}CdWO_4$, and 3.65 and 3.20 for the $CdWO_4$ detectors.

To determine the time resolution of the detector system, we used calibration data collected with a ^{22}Na γ-ray source. ^{22}Na is both a source of 1274.5 keV γ quanta and of positrons. Figure 4 shows the distribution of differences (Δt) between the start of signals in the $^{106}CdWO_4$ and in the $CdWO_4$ detectors with energy $511 \pm 2\sigma_E$ keV, which occur after the positrons annihilation (σ_E is the energy resolution of the $CdWO_4$ counters

for 511-keV γ-quanta). The distribution was approximated by an exponentially modified Gaussian function:

$$f(\Delta t) = A \times \begin{cases} \exp\left(-\frac{1}{2}\left(\frac{\Delta t-\mu}{\sigma}\right)^2\right), & \frac{\Delta t-\mu}{\sigma} \leq k; \\ \exp\left(\frac{k^2}{2} - k\frac{\Delta t-\mu}{\sigma}\right), & \frac{\Delta t-\mu}{\sigma} > k, \end{cases} \quad (2)$$

where A, μ, σ, and k are free parameters of the fit. By analyzing the number of events in the 1274.5 keV peak in coincidence with 511 keV γ-quanta we obtained a selection efficiency of $\eta_{\Delta t} = 92(2)\%$ in the -50 ns $\leq \Delta t < 100$ ns time interval.

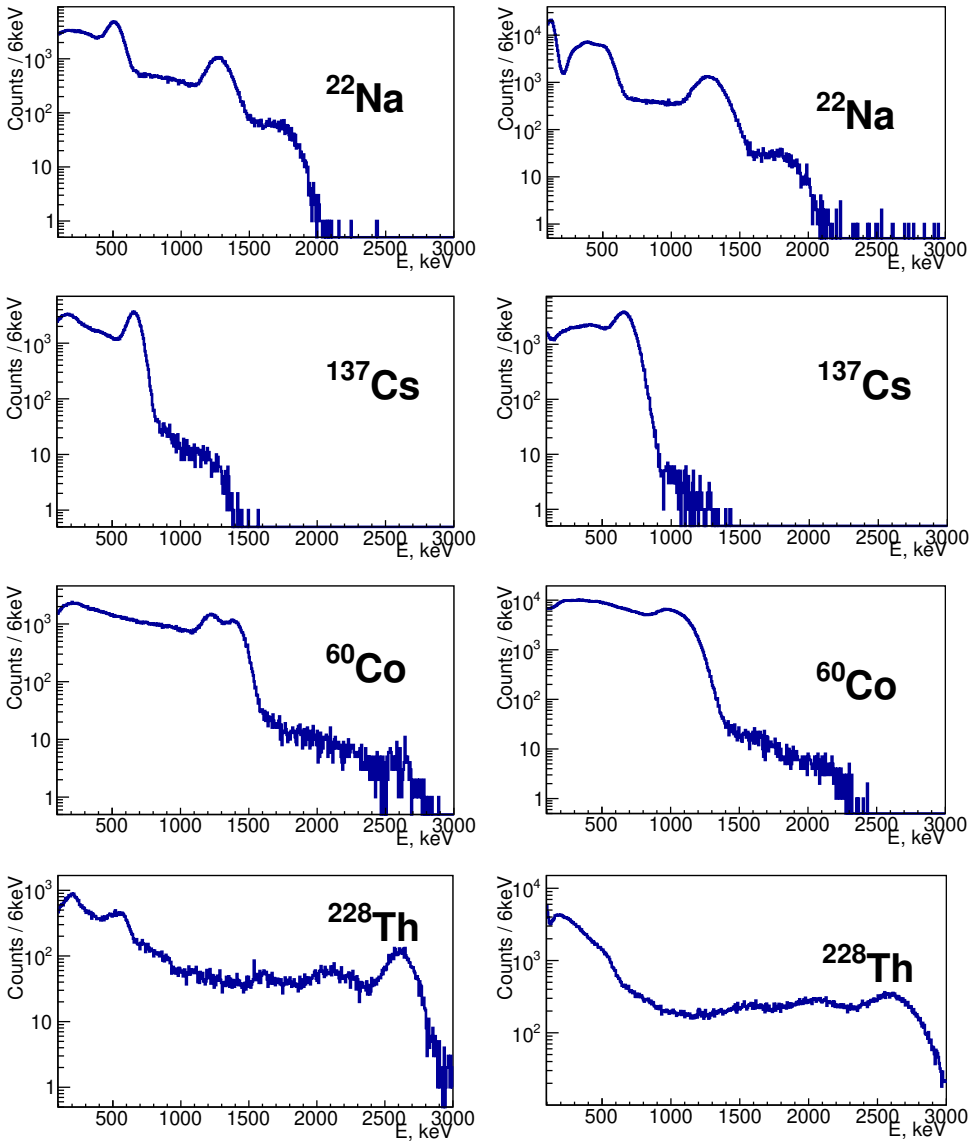

Figure 3. Energy spectra of ^{22}Na, ^{137}Cs, ^{60}Co, and ^{228}Th γ-ray sources measured by one of the $CdWO_4$ (left column) and $^{106}CdWO_4$ (right column) detectors.

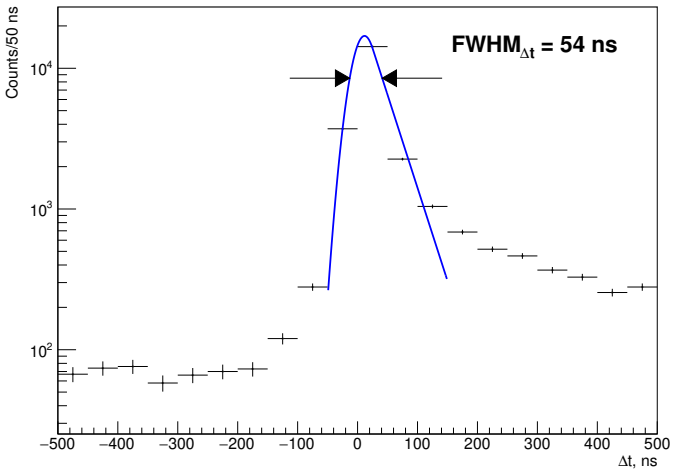

Figure 4. Distribution of the time intervals (Δt) between signals of the $^{106}CdWO_4$ detector and one of the $CdWO_4$ counters with energy $511 \pm 2\sigma_E$ keV, where σ_E is the standard deviation of energy resolution of the $CdWO_4$ counters. The distribution is fitted with an exponentially modified Gaussian function (Equation (2)) with FWHM = 54 ns.

3.2. Pulse-Shape Discrimination

The difference between the pulse shape of $\gamma\&\beta$ and α scintillation signals was used to reject background due to α particles. A numerical characteristic called the Shape Indicator (SI) was calculated for each signal:

$$SI = \sum f(t_k) \times P(t_k) / \sum f(t_k). \quad (3)$$

The weight function $P(t)$ is defined as:

$$P(t) = \{\overline{f}_\alpha(t) - \overline{f}_\gamma(t)\} / \{\overline{f}_\alpha(t) + \overline{f}_\gamma(t)\}, \quad (4)$$

where the reference pulse shapes $\overline{f}_\alpha(t)$ and $\overline{f}_\gamma(t)$ were built by analysing the γ-quanta events from the calibration data and internal α events. More about the pulse-shape discrimination of scintillation signals using the optimal filter method can be found in ref. [41]. The dependence of SI on energy for one of the $CdWO_4$ detectors is shown in Figure 5. As shown, α particles are clearly distinguished from $\gamma\&\beta$. The SI distributions for $\gamma\&\beta$ and α events are well described by a Gaussian function (Figure 5a inset). The mean value (μ_{PSD}) and standard deviation (σ_{PSD}) of the Gaussian function depend on energy (E) as $\mu_{PSD} = p_0 + p_1 \times E + p_2 \times e^{p_3 \times E}$ and $\sigma_{PSD} = p_4/\sqrt{E} + p_5$, where p_i are parameters. For $CdWO_4$ detectors, the selection cut for $\gamma\&\beta$ events is $\mu_{PSD} \pm 3 \times \sigma_{PSD}$, which gives the selection efficiency $\eta_{SI}^{nat} = 99.7\%$, while for α events it is $\mu_{PSD} \pm 2 \times \sigma_{PSD}$. For the $^{106}CdWO_4$ detectors the selection cut is more complex: $\mu_{PSD}{}^{+3\times\sigma_{PSD}}_{-1.5\times\sigma_{PSD}}$ for events with $E < 1500$ keV ($\eta_{SI}^{106} = 93.2\%$) and $\mu_{PSD} \pm 3 \times \sigma_{PSD}$ for events with $E > 1500$ keV ($\eta_{SI}^{106} = 99.7\%$). This choice of selection conditions was made due to the worse discrimination between the $\gamma\&\beta$ and α signals exhibited by the $^{106}CdWO_4$ detector [40].

It is worth noting that the energy of α particles (E_α) which belong to the U/Th families is 5.7–6.9 MeV. Due to the quenching of α particles in the γ scale, the α spectrum is shifted to lower energies [42]. A dependence of the α/γ ratio (i.e., ratio of energy of α particle in γ scale to its real energy) was determined for the $^{106}CdWO_4$ detector as $\alpha/\gamma = 0.12(2) + 0.011(2) \times E_\alpha$ and for $CdWO_4$ detectors as $\alpha/\gamma = 0.08(1) + 0.015(2) \times E_\alpha$, where E_α is in MeV [40]. Also, the analysis of α spectra made it possible to determine the contamination of crystals by α-active daughter nuclides of the U/Th chains [40].

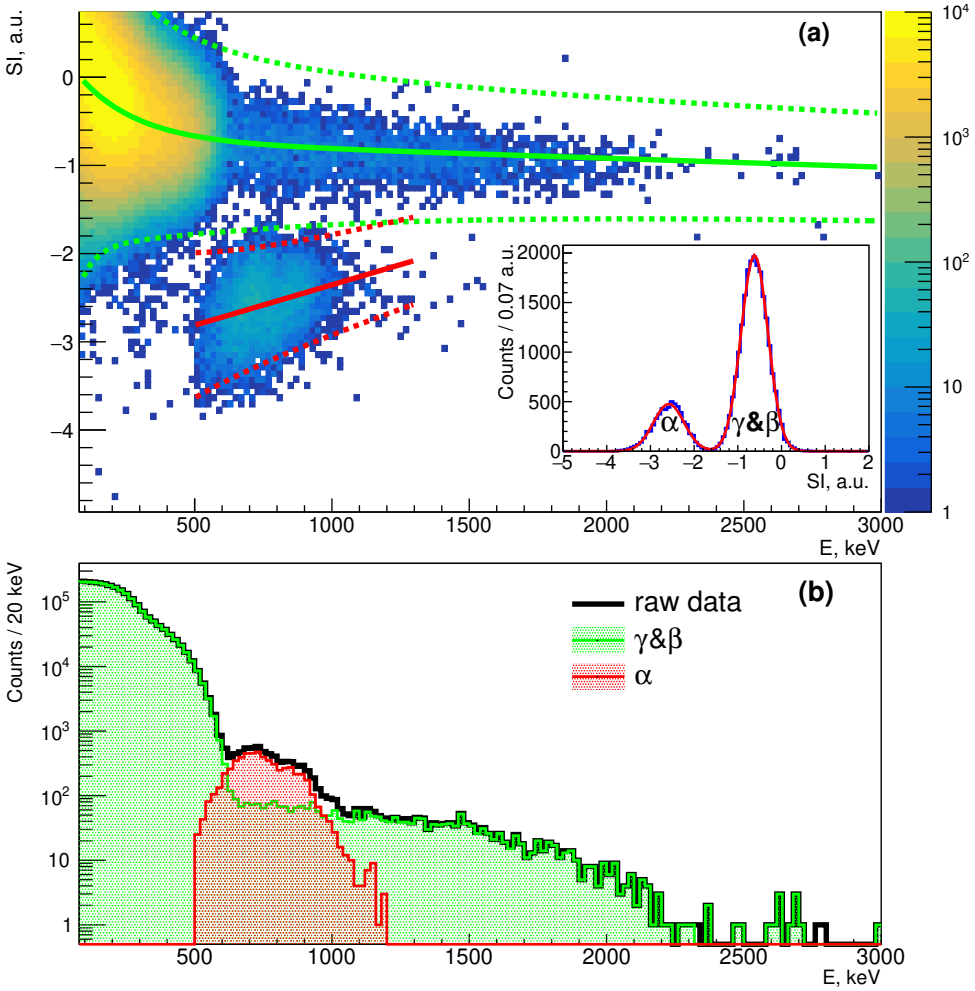

Figure 5. Two-dimensional distribution of the background events measured by $CdWO_4$ detector in energy (E) versus Shape Indicator (SI) coordinates (**a**). Distributions of the SI parameters for $\gamma\&\beta$ and α particles approximated by two Gaussian functions in the energy interval 500–1200 keV (inset in (**a**)). The green and red solid lines in the panel (**a**) represent μ_{PSD} for $\gamma\&\beta$ and α events, respectively. The green and red dashed lines in the panel (**a**) represent $\mu_{PSD} \pm 3 \times \sigma_{PSD}$ for $\gamma\&\beta$ events and $\mu_{PSD} \pm 2 \times \sigma_{PSD}$ for α events. Selected α and $\gamma\&\beta$ events between the dashed lines projected on the energy axis are shown in the panel (**b**).

3.3. Experimental Energy Spectra

The experimental energy spectra measured over 1075 days by the $^{106}CdWO_4$ and $CdWO_4$ detectors under different selection conditions are shown in Figure 6. It was possible to achieve a noticeable reduction of the background measured by the $^{106}CdWO_4$ detector in the energy range of 0.5–1.5 MeV by separating $\gamma\&\beta$ events from α ones by the pulse-shape discrimination. The main part of the spectrum measured by the $^{106}CdWO_4$ detector with energy < 0.5 MeV in anti-coincidence (AC) with the $CdWO_4$ counters is the ^{113m}Cd β distribution. For the events in coincidence (CC) with the $CdWO_4$ counters, the data acquisition system records events with the low energy trigger of the $^{106}CdWO_4$ detector (see Section 2). As a result, the ^{113m}Cd β spectrum represents the main part of the spectra for all the detectors below 0.5 MeV. Also, an important selection condition is a coincidence with 511 keV γ-quantum (quanta) in the $CdWO_4$ counter(s), which should occur during the annihilation of a positron from the double beta processes in ^{106}Cd with positron(s) emission (Figure 6, $\gamma\&\beta$ CC $E^{nat} = 511 \pm 2\sigma_E$ keV, where E^{nat} is an energy deposit in at least one of $CdWO_4$ detectors). The only two peaks with energies of 202 keV and 307 keV that can be seen in the spectrum measured by the $CdWO_4$ counters in coincidence with events in the

$^{106}CdWO_4$ detector with energy above 500 keV (Figure 6, $\gamma\&\beta$ CC $E^{106} > 500$ keV, where E^{106} is an energy deposit in $^{106}CdWO_4$ detector) correspond to the β decay of ^{176}Lu.

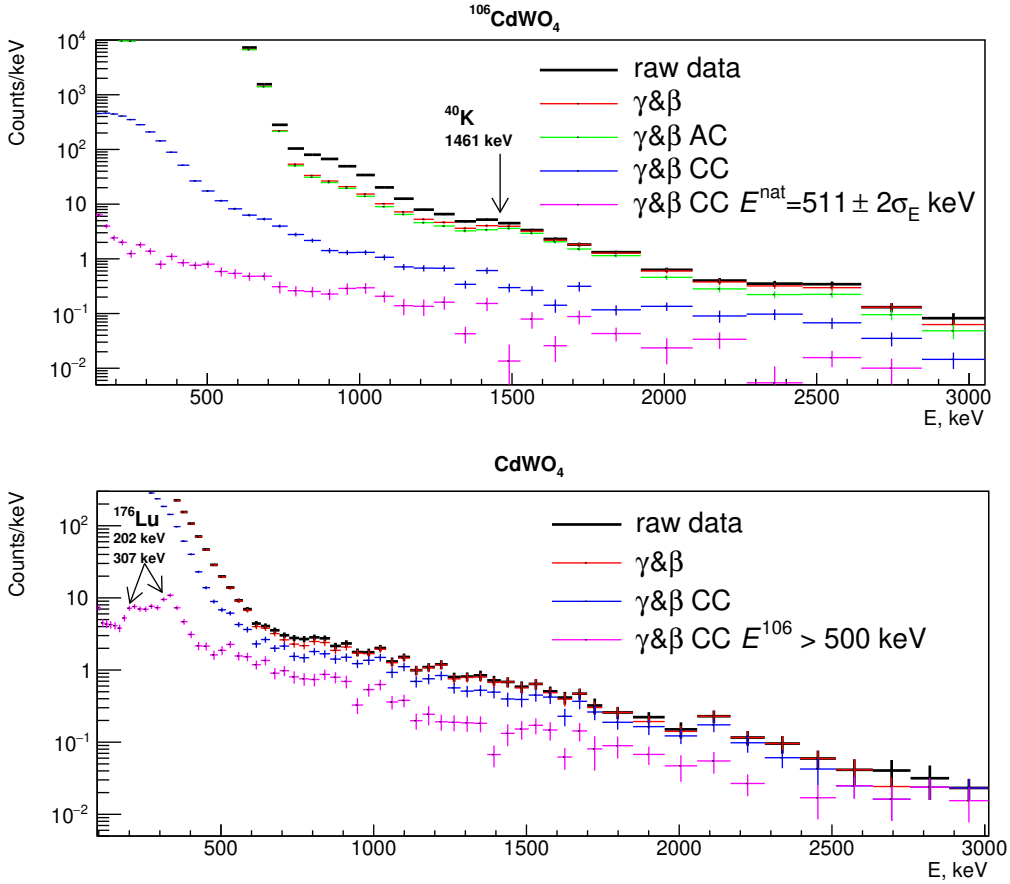

Figure 6. Energy spectra measured by $^{106}CdWO_4$ (**top**) and both $CdWO_4$ detectors (**bottom**) for 1075 days under the different selection conditions. $\gamma\&\beta$ denotes spectrum of $\gamma\&\beta$-events. AC (CC) means anti-coincidence (coincidence) mode, respectively. $E^{nat} = 511 \pm 2\sigma_E$ keV denotes energy deposit in at least one of the $CdWO_4$ detectors in the energy interval $511 \pm 2\sigma_E$ keV, where σ_E is the standard deviation of energy resolution. $E^{106} > 500$ keV denotes energy deposit in $^{106}CdWO_4$ detector more than 500 keV. The bin width is proportional to the energy resolution.

3.4. Radioactive Contamination of the Experimental Setup

To describe the experimental data measured by the $^{106}CdWO_4$ detector above 0.8 MeV in AC and above 0.4 MeV in CC, a background model was constructed from the following components:

(1) ^{40}K and ^{232}Th, ^{238}U with their daughters in all the setup components;
(2) Residual α distribution in the $^{106}CdWO_4$ crystal (7.3% of the alpha distribution);
(3) Beta decay of ^{176}Lu and ^{113m}Cd, and $2\nu2\beta$ decay of ^{116}Cd with a half-life of $T_{1/2} = 2.63 \times 10^{19}$ years in the $^{106}CdWO_4$ crystal scintillator. The number of ^{116}Cd $2\nu2\beta$ decays in the experimental spectra is well known due to the known isotopic concentration of ^{116}Cd in the $^{106}CdWO_4$ crystal [36];
(4) ^{113}Cd in the $CdWO_4$ and $^{106}CdWO_4$ crystal scintillators;
(5) ^{56}Co and ^{60}Co in the internal copper.

The secular equilibrium of the ^{232}Th and ^{238}U chains is assumed to be broken due to physical and chemical processes utilized for the production of the experimental setup materials. Therefore, the following sub-chains were considered separately: $^{228}Ra \longrightarrow {}^{228}Th$

and ^{228}Th $\longrightarrow$ ^{208}Pb (the ^{232}Th chain); ^{238}U $\longrightarrow$ ^{234}U, ^{226}Ra $\longrightarrow$ ^{210}Pb and ^{210}Pb $\longrightarrow$ ^{206}Pb (the ^{238}U chain).

The energy distributions of the background components were simulated using the Monte Carlo package EGSnrc [43] with the initial kinematics provided by the DECAY0 event generator [44]. Each distribution was properly normalized by the parameter representing the number of decays. This parameter is obtained through fitting the experimental data by the Monte Carlo simulated distributions. The spectral shape of the distributions account also for the SI and Δt selection cuts that were applied to the data. Each simulated event was multiplied by η_{SI} and $\eta_{\Delta t}$. Figure 7 shows the result of the simultaneous binned maximum likelihood fit of five $\gamma\&\beta$ spectra: three spectra measured by the $^{106}CdWO_4$ detector under selection conditions AC, CC, and CC $E^{\text{nat}} = 511 \pm 2\sigma_E$ keV; and two spectra measured by the $CdWO_4$ detectors under the selection conditions CC and CC $E^{106} > 500$ keV. The maximum likelihood was applied since many bins have very low data statistics. The goodness of the fit is calculated with the Baker–Cousins approach [45] $\chi^2/NDF = 421/123 = 3.4$, where NDF is a number of degrees of freedom. The fit quality is rather low. However, the problem may be that one cannot be sure all the contaminations of the set-up materials are included in the background model. Moreover, despite efforts to reconstruct the setup geometry in the Monte Carlo simulations as accurately as possible, it does not perfectly reproduce the actual experiment's geometry. Some worsening of the fit quality could also be due to imperfect knowledge of the detector system's spectrometric characteristics, their degradation in time, etc. The radioactive contaminations of the main components of the experimental setup are reported in Table 1. The ^{228}Th contaminations in the $^{106}CdWO_4$ and in $CdWO_4$ detectors were determined by using the time-amplitude analysis [40]. Activities of ^{238}U, ^{234}U, ^{230}Th, ^{226}Ra, ^{210}Pb, and ^{232}Th in the $CdWO_4$ detectors were determined by the α spectrum analysis [40].

Table 1. Radioactive contamination (mBq/kg) of the setup details. Upper limits are given at 90% confidence level, uncertainties of the last digit are given with 68% confidence level. Activities labeled by (*) were determined by using the time-amplitude analysis, the values marked by (†) were determined by analysis of the α distribution [40]. Q. lg. denotes quartz light guide.

Setup Component	^{238}U	^{234}U	^{230}Th	^{226}Ra	^{210}Pb	^{232}Th	^{228}Ra	^{228}Th	^{40}K	^{176}Lu	^{56}Co	^{60}Co
$^{106}CdWO_4$	0.65(3)			<0.04	<0.4		<0.02	0.0174(14) *	<0.24	1.68(3)		
$CdWO_4$	0.29(7) †	<0.2 †	1.40(7) †	<0.002 †	0.89(4) †	<0.01 †	<0.03	0.012(2) *	<2			
Plastic scintillator	<8.9			<1.1	<11.8		<2.8	<1.1	<8.7			
Optical couplant	<59			<79	<32		<13	<9.5	<260			
Teflon tape	<4.1			<2.0	<31		<6.4	<2.8	<12			
Teflon support details	<1.4			<1.3	<7.3		<5.0	<5.2	<9.7			
Q. lg. for $CdWO_4$	<1.0			<3.4	<3.2		<0.6	<0.4	<1.2			
Q. lg. for $^{106}CdWO_4$	<3.5			<9.3	<20		<9.1	<14.7	<40			
Internal copper	<4.2			<0.09	<28		<0.16	<0.04	<2.4		<0.08	<0.07
External copper	<17			<0.46			<0.39	<0.08	<0.73			
PMTs for $CdWO_4$	<920			<1530			<1500	<1420	<1630			
PMTs for $^{106}CdWO_4$	<1400			<2500			<2500	<450	<2320			

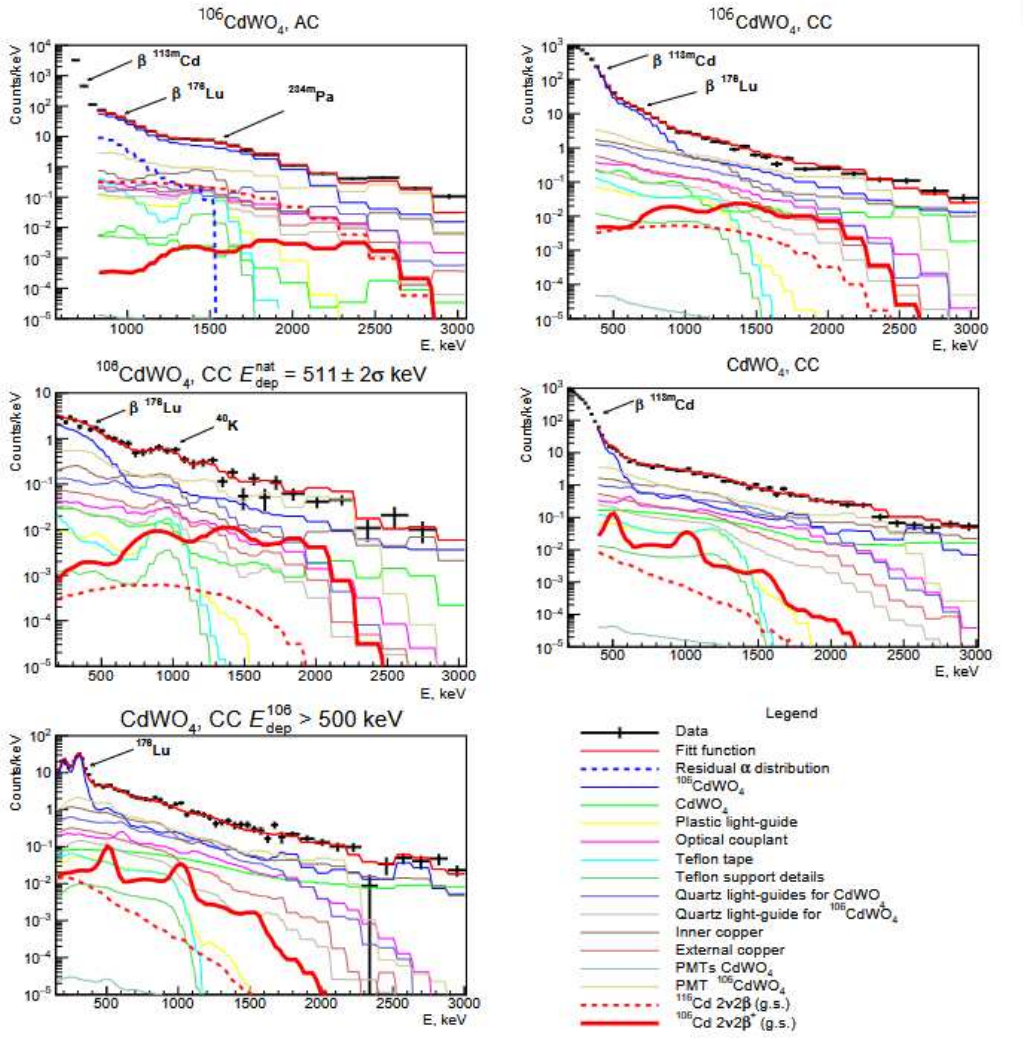

Figure 7. Results of the combined approximation of the $\gamma\&\beta$ spectra measured by the $^{106}CdWO_4$ and two $CdWO_4$ detectors under different selection conditions (see Section 3.3). The fit function represents the approximation result. The contributions from the contamination of the setup details are shown separately (see legend). An excluded distribution of the $2\nu2\beta^+$ decay of ^{106}Cd to the ground state of ^{106}Pd with a half-life $T_{1/2} = 1.7 \times 10^{22}$ years is shown by solid red line in all the spectra.

4. Half-Life Limits on 2β Decay Processes in ^{106}Cd

There were no peculiarities in the experimental data that could be attributed to the 2β decay of ^{106}Cd. Therefore, half-life limits for different channels and modes of 2β decay were set using the formula:

$$\lim T_{1/2} = N(^{106}\mathrm{Cd}) \times \ln 2 \times t \times \eta_{\mathrm{det}} \times \eta_{\mathrm{sel}} \times t / \lim S, \quad (5)$$

where $N(^{106}\mathrm{Cd}) = 2.42 \times 10^{23}$ is the number of ^{106}Cd nuclei in the $^{106}CdWO_4$ crystal, η_{det} and η_{sel} are detection and selection efficiencies, t is the measurement live time, and $\lim S$ is a number of events of the effect searched for that can be excluded with a given confidence level (C.L.). Values of $\lim S$ depend on selection conditions and can be obtained from the approximation of the experimental energy spectrum with a background model plus an effect searched for. For simultaneous approximation of several spectra, the Equation (5)

must be modified. Since the spectral shape of the Monte Carlo distributions account for the parameters η_{det} and η_{sel}, Equation (5) can be rewritten as:

$$\lim T_{1/2} = N(^{106}\mathrm{Cd}) \times \ln 2 \times t / \lim N_{dec}, \quad (6)$$

where $\lim N_{dec} = \lim S/(\eta_{det} \times \eta_{sel})$ is a number of decays of the process searched for. Now, values of $\lim N_{dec}$ can be obtained from simultaneous approximation of the energy spectra with different selection conditions. The parameters of the approximation were bounded, taking into account the data on the radioactive contamination of the experimental setup details (see Table 1).

For example, for the $2\nu2\beta^+$ decay of ^{106}Cd to the ground state of ^{106}Pd, the fit gives $N_{dec} = 0 \pm 18$. According to [46], we took $\lim N_{dec} = 29$ events at 90% C.L., which gives $\lim T_{1/2}^{2\nu2\beta^+ g.s.} = 1.7 \times 10^{22}$ years (the distribution is shown in Figure 7). The total detection efficiency for $2\nu2\beta^+$ decay to the ground state of ^{106}Pd for the different selection conditions and detectors are: $\eta_{AC}^{106} = 12.8\%$, $\eta_{CC}^{106} = 79.6\%$, $\eta_{CCE^{nat}=511\pm2\sigma_E keV}^{106} = 37.3\%$, $\eta_{CC}^{nat} = 52.7\%$, and $\eta_{CCE^{106}>500keV}^{nat} = 49.1\%$. The half-life limits on different modes of 2β decay of ^{106}Cd were obtained in a similar way and are presented in Table 2.

One of the most interesting processes is $2\nu EC\beta^+$ decay of ^{106}Cd to the ground state of ^{106}Pd. In this work, we give a new half-life limit on this process as $\lim T_{1/2}^{2\nu EC\beta^+ g.s.} = 7.7 \times 10^{21}$ years, which is in the region of the theoretical prediction $T_{1/2} = 10^{21} - 10^{23}$ years [47–53]. The most optimistic theoretical calculations $T_{1/2} = 10^{20} - 10^{22}$ years are for $2\nu2EC$ decay to the ground state of ^{106}Pd. But due to the large background from the β decays of ^{113m}Cd and ^{113}Cd, it is difficult to obtain a high-sensitivity search for the characteristic X-rays from $2\nu2EC$ decay that are expected in the low energy region.

Another interesting feature is the possibility of near resonant $0\nu2EC$ decays of ^{106}Cd to excited levels of ^{106}Pd when the initial and final states are degenerate [32]. There are three possible near resonant transitions to the 2718 keV, 2741 keV, and 2748 keV excited levels of ^{106}Pd. In this work we give the half-life limits on the near resonance processes as $\lim T_{1/2}^{Res.0\nu2EC} = (1.2 - 2.0) \times 10^{21}$ years (see Table 2).

Table 2. Half-life limits on different modes and channels of 2β decay of ^{106}Cd given at 90% confidence level. The most sensitive previous results and the theoretical predictions are also presented.

Decay	Level of ^{106}Pd, keV	Theoretical $T_{1/2}$, Years	$\lim T_{1/2}$, Years	
			Previous Result	Present Work
$2\nu2\beta^+$	g.s.	$(5.4 - 880) \times 10^{25}$ [47,48,50], $>2.4 \times 10^{27}$ [49]	4.4×10^{21} [54]	1.7×10^{22}
	512	$(1.5 - 25) \times 10^{27}$ [47,55,56]	4.1×10^{21} [54]	1.5×10^{22}
$0\nu2\beta^+$	g.s.	$(1.4 - 32) \times 10^{27}$ [47,55–61]	5.9×10^{21} [62]	2.2×10^{22}
	512		4.1×10^{21} [54]	1.5×10^{22}
$2\nu EC\beta^+$	g.s.	$(1.4 - 240) \times 10^{21}$ [47,48,50–53], $>2.7 \times 10^{22}$ [49]	2.1×10^{21} [62]	7.7×10^{21}
	512	$(5.3 - 24) \times 10^{25}$ [51,52], $>1.1 \times 10^{25}$ [49]	3.3×10^{21} [54]	9.9×10^{21}
	1128	3.7×10^{30} [51]	2.0×10^{21} [54]	1.2×10^{22}
	1134	$(1.3 - 13) \times 10^{26}$ [51,52], $>1.1 \times 10^{27}$ [49]	2.5×10^{21} [54]	1.3×10^{22}
$0\nu EC\beta^+$	g.s.	$(1.0 - 17) \times 10^{26}$ [32,47,55,56]	1.4×10^{22} [62]	1.5×10^{22}
	512		9.7×10^{21} [62]	2.1×10^{22}
	1128		1.0×10^{22} [62]	1.9×10^{22}
	1134	$(1.0 - 21) \times 10^{29}$ [32,55,57,58]	2.7×10^{21} [54]	2.1×10^{22}

Table 2. *Cont.*

Decay	Level of ^{106}Pd, keV	Theoretical $T_{1/2}$, Years	lim$T_{1/2}$, Years	
			Previous Result	Present Work
2ν2EC	g.s.	$(2.0-230)\times10^{20}$ [47,48,50–53]	1.7×10^{21} [63]	–
	512	$(1.5-9.4)\times10^{27}$ [51,52], $>4.0\times10^{26}$ [49]	9.9×10^{20} [64]	2.2×10^{20}
	1128	9.9×10^{28} [51]	6.6×10^{20} [62]	9.3×10^{20}
	1134	$(1.1-11)\times10^{23}$ [51,52]	1.0×10^{21} [64]	1.4×10^{21}
	1562	$(2.4-4.3)\times10^{28}$ [52], $>5.4\times10^{28}$ [49]	7.8×10^{20} [62]	7.9×10^{20}
	1706	$>1.9\times10^{25}$ [49]	7.1×10^{20} [64]	4.6×10^{21}
	2001	$>8.9\times10^{24}$ [49]	1.5×10^{21} [62]	1.4×10^{21}
	2278	$>2.1\times10^{27}$ [49]	1.0×10^{21} [64]	1.8×10^{21}
0ν2EC	g.s.		1.0×10^{21} [39]	1.2×10^{21}
	512		5.1×10^{20} [39]	1.9×10^{21}
	1128		5.1×10^{20} [64]	1.7×10^{21}
	1134		1.1×10^{21} [64]	2.2×10^{21}
	1562		1.4×10^{21} [62]	2.0×10^{21}
	1706		2.0×10^{21} [62]	1.7×10^{21}
	2001		1.2×10^{21} [64]	3.3×10^{21}
	2278		1.2×10^{21} [62]	1.2×10^{21}
Res. 0ν2EC	2718	$(3.2-9.7)\times10^{22}$ [57], $>5.2\times10^{24}$ [65,66], $>7.9\times10^{23}$ [32]	2.9×10^{21} [62]	2.0×10^{21}
	2741	$>5.2\times10^{24}$ [66]	9.5×10^{20} [39]	1.2×10^{21}
	2748	$2\times10^{29}-2\times10^{34}$ [29]	1.4×10^{21} [64]	1.9×10^{21}

5. Conclusions

One of the most sensitive double beta plus experiments to search for 2β decay of ^{106}Cd with an enriched $^{106}CdWO_4$ scintillator in coincidence with two large volume $CdWO_4$ counters was carried out at the Gran Sasso underground laboratory of the INFN (Italy). After 1075 days of data taking, we were able to provide new improved half-life limits on the different channels and modes of ^{106}Cd 2β decay at the level of lim $T_{1/2} = 10^{20}$–10^{22} years. A new half-life limit on 2νECβ^+ decay to the ground state of ^{106}Pd was set as lim $T_{1/2}^{2\nu EC\beta^+ g.s.} = 7.7\times10^{21}$ years, in the region of the theoretical predictions of 10^{21}–10^{23} years. The half-life limits on near resonant 0ν2EC decay transitions to the 2718 keV, 2741 keV, and 2748 keV excited levels of ^{106}Pd have been set at the level lim $T_{1/2}^{Res.0\nu2EC} = (1.2-2.0)\times10^{21}$ years. Analysis of the complete data set of the experiment is in progress.

Author Contributions: Conceptualization, P.B., R.B. and F.A.D.; Data curation, P.B., V.C., R.C., A.L. and O.G.P.; Formal analysis, F.C., F.A.D., V.R.K. and A.L.; Funding acquisition, P.B., R.B., F.A.D. and V.V.K.; Investigation, P.B., R.B., V.C., R.C., F.A.D., A.I., D.V.K., V.R.K., A.L., O.G.P. and V.I.T.; Methodology, P.B., R.B. and F.A.D.; Project administration, P.B., R.B., F.A.D. and V.V.K.; Resources, P.B., R.B. and F.A.D.; Software, P.B., F.C., V.C., R.C., F.A.D., V.R.K. and V.I.T.; Supervision, P.B., R.B. and F.A.D.; Validation, P.B., R.B., F.C., F.A.D., V.R.K. and V.I.T.; Visualization, F.C., F.A.D. and V.R.K.; Writing—original draft, V.R.K.; Writing—review & editing, P.B., R.B., F.C., V.C., R.C., F.A.D., A.I., D.V.K., V.V.K., A.L., V.M., O.G.P. and V.I.T. All authors have read and agreed to the published version of the manuscript.

Funding: V.R.K., D.V.K., V.V.K. and O.G.P. were supported in part by the National Research Foundation of Ukraine (Grant No. 2023.03/0213). V.R.K. and D.V.K. were supported in part by the project "Study of double beta decay of 106Cd and 116Cd with scintillators from enriched isotopes" of the program of the National Academy of Sciences of Ukraine "Research of young scientists of the National Academy of Sciences of Ukraine in 2023–2024"

Data Availability Statement: The data produced in this study are contained in the publication.

Acknowledgments: F.A. Danevich, O.G. Polischuk, and V.I. Tretyak thank the INFN and the people of the DAMA group for the great support and kind hospitality in the present difficult times; moreover, all the Ukrainian authors express great gratitude to the Armed Forces of Ukraine, which defend the independence of the country and protect the lives of its citizens from the present Russian aggression.

Conflicts of Interest: The authors declare no conflicts of interest.

References

1. Bilenky, S. *Introduction to the Physics of Massive and Mixed Neutrinos*; Springer: Berlin/Heidelberg, Germany, 2018.
2. Qian, X.; Vogel, P. Neutrino mass hierarchy. *Prog. Part. Nucl. Phys.* **2015**, *83*, 1–30.
3. Fukugita, M.; Yanagida, T. Baryogenesis without Grand Unification. *Phys. Lett. B* **1986**, *174*, 45–47. [CrossRef]
4. Davidson, S.; Nardi, E.; Nir, Y. Leptogenesis. *Phys. Rept.* **2008**, *466*, 105–177.
5. Branco, G.C.; Gonzalez Felipe, R.; Joaquim, F.R. Leptonic CP violation. *Rev. Mod. Phys.* **2012**, *84*, 515–565.
6. Blanchet, S.; Di Bari, P. The minimal scenario of leptogenesis. *New J. Phys.* **2012**, *14*, 125012.
7. Deppisch, F.F.; Graf, L.; Harz, J.; Huang, W.-C. Neutrinoless double beta decay and the baryon asymmetry of the Universe. *Phys. Rev. D* **2018**, *98*, 055029.
8. Gomez-Cadenas, J.J.; Martin-Albo, J.; Menendez, J.; Mezzetto, M.; Monrabal, F.; Sorel, M. The search for neutrinoless double-beta decay. *Riv. Nuovo Cim.* **2023**, *46*, 619–692.
9. Agostini, M.; Benato, G.; Detwiler, J.A.; Menendez, J.; Vissani, F. Toward the discovery of matter creation with neutrinoless $\beta\beta$ decay. *Rev. Mod. Phys.* **2023**, *95*, 025002.
10. Bossio, E.; Agostini, M. Probing beyond the standard model physics with double-beta decays. *J. Phys. G* **2024**, *51*, 023001.
11. Parno, D.S.; Poon, A.W.P.; Singh, V. Experimental neutrino physics in a nuclear landscape. *Phil. Trans. R. Soc. A* **2024**, *382*, 20230122.
12. Dolinski, M.J.; Poon, A.W.P; Rodejohann, W. Neutrinoless Double-Beta Decay: Status and Prospects. *Annu. Rev. Nucl. Part. Sci.* **2019**, *25*, 19–51.
13. Schechter, J.; Valle, J.W.F. Neutrinoless double-β decay in SU(2) $\times$ U(1) theories. *Phys. Rev. D* **1982**, *25*, 2951–2954. [CrossRef]
14. Saakyan, R. Two-Neutrino Double-Beta Decay. *Annu. Rev. Nucl. Part. Sci.* **2013**, *63*, 503–529.
15. Pritychenko, B.; Tretyak, V.I. Comprehensive review of 2β decay half-lives. *At. Data Nucl. Data Tables* **2025**, *161*, 101694. [CrossRef]
16. Gavrilyuk, Y.M.; Gangapshev, A.M.; Kazalov, V.V.; Kuzminov, V.V.; Panasenko, S.I.; Ratkevich, S.S. Indications of $2\nu2K$ capture in ^{78}Kr. *Phys. Rev. C* **2013**, *87*, 035501. [CrossRef]
17. Meshik, A.P.; Hohenberg, C.M.; Pravdivtseva, O.V.; Kapusta, Y.S. Weak decay of ^{130}Ba and ^{132}Ba: Geochemical measurements. *Phys. Rev. C* **2001**, *64*, 035205.
18. Pujol, M.; Marty, B.; Burnard, P.; Philippot, P. Xenon in Archean barite: Weak decay of ^{130}Ba, mass-dependent isotopic fractionation and implication for barite formation. *Geochim. Cosmochim. Acta* **2009**, *73*, 6834–6846.
19. Aprile, E. et al. [XENON Collaboration] Search for New Physics in Electronic Recoil Data from XENONnT. *Phys. Rev. Lett.* **2022**, *129*, 161805.
20. Aalbers, J.; et al. [LZ Collaboration] Two-neutrino double electron capture of ^{124}Xe in the first LUX-ZEPLIN exposure. *J. Phys. G* **2025**, *52*, 015103.
21. Bo, Z. et al. [PandaX Collaboration] Search for Majorana Neutrinos with the Complete KamLAND-Zen Dataset. *arXiv* **2024**, arXiv:2411.14355.
22. Abe, S. et al. [KamLAND-Zen Collaboration] Search for Majorana Neutrinos with the Complete KamLAND-Zen Dataset. *arXiv* **2024**, arXiv:2406.11438.
23. Adams, D.Q. et al. [CUORE Collaboration] With or without ν? Hunting for the seed of the matter-antimatter asymmetry. *arXiv* **2024**, arXiv:2404.04453.
24. Agrawal, A. et al. [AMoRE Collaboration] Improved limit on neutrinoless double beta decay of ^{100}Mo from AMoRE-I. *Phys. Rev. Lett.* **2025**, *134*, 082501.
25. Agostini, M. et al. [GERDA Collaboration] Final Results of GERDA on the Search for Neutrinoless Double-β Decay. *Phys. Rev. Lett.* **2020**, *125*, 252502.
26. Arnquist, I.J. et al. [Majorana Collaboration] Final Result of the MAJORANA DEMONSTRATOR's Search for Neutrinoless Double-β Decay in ^{76}Ge. *Phys. Rev. Lett.* **2023**, *130*, 062501.
27. Abgrall, N. et al. [LEGEND Collaboration] LEGEND-1000 Preconceptual Design Report. *arXiv* **2021**, arXiv:2107.11462.
28. Hirsch, M.; Muto, K.; Oda, T.; Klapdor-Kleingrothaus, H.V. Nuclear structure calculation of $\beta^+\beta^+$, β^+/EC and EC/EC decay matrix elements. *Z. Phys. A* **1994**, *347*, 151–160.
29. Blaum, K.; Eliseev, S.; Danevich, F.A.; Tretyak, V.I.; Kovalenko, S.; Krivoruchenko, M.I.; Novikov, Y.N.; Suhonen, J. Neutrinoless double-electron capture. *Rev. Mod. Phys.* **2020**, *92*, 045007.

30. Winter, R. Double *K* Capture and Single *K* Capture with Positron Emission. *Phys. Rev.* **1955**, *100*, 142–144.
31. Bernabeu, J.; De Rujula, A.; Jarlskog, C. Neutrinoless double electron capture as a tool to measure the electron neutrino mass. *Nucl. Phys. B* **1983**, *223*, 15–28.
32. Suhonen, J. Neutrinoless double beta decays of ^{106}Cd revisited. *Phys. Lett. B* **2011**, *701*, 490–495. [CrossRef]
33. Wang, M.; Huang, W.J.; Kondev, F.G.; Audi, G.; Naimi, S. The AME 2020 atomic mass evaluation (II). Tables, graphs and references. *Chin. Phys. C* **2021**, *45*, 030003. [CrossRef]
34. Meija, J.; Coplen, T.B.; Berglund, M.; Brand, W.A.; De Bievre, P.; Groning, M.; Holden, N.E.; Irrgeher, J.; Loss, R.D.; Walczyk, T.; et al. Isotopic compositions of the elements 2013 (IUPAC Technical Report). *Pure Appl. Chem.* **2016**, *88*, 293–306. [CrossRef]
35. Barabash, A.S.; Belli, P.; Bernabei, R.; Boiko, R.S.; Cappella, F.; Caracciolo, V.; Chernyak, D.M.; Cerulli, R.; Danevich, F.A.; Di Vacri, M.L.; et al. Low background detector with enriched $^{116}CdWO_4$ crystal scintillators to search for double beta decay of ^{116}Cd. *JINST* **2011**, *6*, P08011. [CrossRef]
36. Belli, P.; Bernabei, R.; Boiko, R.S.; Brudanin, V.B.; Bukilic, N.; Cerulli, R.; Chernyak, D.M.; Danevich, F.A.; D'Angelo, S.; Degoda, V.Y.; et al. Development of enriched $^{106}CdWO_4$ crystal scintillators to search for double beta decay processes in ^{106}Cd. *Nucl. Instrum. Meth. A* **2010**, *615*, 301–306. [CrossRef]
37. Bernabei, R.; Belli, P.; Cappella, F.; Cerulli, R.; Dai, C.J.; D'Angelo, A.; He, H.L.; Incicchitti, A.; Kuang, H.H.; Ma, J.M.; et al. First results from DAMA/LIBRA and the combined results with DAMA/NaI. *Eur. Phys. J. C* **2008**, *56*, 333–355. [CrossRef]
38. Bardelli, L.; Bini, M.; Bizzeti, P.G.; Carraresi, L.; Danevich, F.A.; Fazzini, T.F.; Grinyov, B.V.; Ivannikova, N.V.; Kobychev, V.V.; Kropivyansky, B.N.; et al. Further study of $CdWO_4$ crystal scintillators as detectors for high sensitivity 2β experiments: Scintillation properties and pulse-shape discrimination. *Nucl. Instrum. Meth. A* **2006**, *569*, 743–753. [CrossRef]
39. Belli, P.; Bernabei, R.; Boiko, R.S.; Brudanin, V.B.; Cappella, F.; Caracciolo, V.; Cerulli, R.; Chernyak, D.M.; Danevich, F.A.; D'Angelo, S.; et al. Search for double-β decay processes in ^{106}Cd with the help of a $^{106}CdWO_4$ crystal scintillator. *Phys. Rev. C* **2012**, *85*, 044610.
40. Belli, P.; Bernabei, R.; Cappella, F.; Caracciolo, V.; Cerulli, R.; Danevich, F.A.; Inchicchitti, A.; Kasperovych, D.V.; Klavdiienko, V.R.; Kobychev, V.V.; et al. Low-background experiment to search for double beta decay of ^{106}Cd using $^{106}CdWO_4$ scintillator. *Nucl. Phys. At. Energy* **2023**, *24*, 193–208. [CrossRef]
41. Danevich, F.A.; Georgadze, A.S.; Kobychev, V.V.; Kropivyansky, B.N.; Nikolaiko, A.S.; Ponkratenko, O.A.; Tretyak, V.I.; Zdesenko, S.Y.; Zdesenko, Y.G.; Bizzeti, P.G.; et al. Search for 2β decay of cadmium and tungsten isotopes: Final results of the Solotvina experiment. *Phys. Rev. C* **2003**, *68*, 035501. [CrossRef]
42. Tretyak, V.I. Semi-empirical calculation of quenching factors for ions in scintillators. *Astropart. Phys.* **2010**, *33*, 40–53.
43. Kawrakow, I.; Mainegra-Hing, E.; Rogers, D.W.O.; Tessier, F.; Walters, B.R.B. *The EGSnrc Code System: Monte Carlo Simulation of Electron and Photon Transport*; NRC: Ottawa, ON, Canada, 2023; 321p.
44. Ponkratenko, O.A.; Tretyak, V.I.; Zdesenko, Y.G. Event generator DECAY4 for simulating double-beta processes and decays of radioactive nuclei. *Phys. At. Nucl.* **2000**, *63*, 1282–1287. [CrossRef]
45. Baker, S.; Cousins, R.D. Clarification of the use of chi-square and likelihood functions in fits to histograms. *Nucl. Instrum. Meth.* **1984**, *221*, 437–442.
46. Feldman, G.J.; Cousins, R.D. Unified approach to the classical statistical analysis of small signals. *Phys. Rev. D* **1998**, *57*, 3873–3889. [CrossRef]
47. Stoica, S.; Klapdor-Kleingrothaus, H.V. $\beta^-\beta^-$, $\beta^+\beta^+$, β^+/EC and EC/EC half-lives for ^{106}Cd within a second QRPA method. *Eur. Phys. J. A* **2003**, *17*, 529–536. [CrossRef]
48. Shukla, A.; Raina, P.K.; Chandra, R.; Rath, P.K.; Hirsch, J.G. Two neutrino positron double beta decay of ^{106}Cd for $0^+ \rightarrow 0^+$ transition. *Eur. Phys. J. A* **2005**, *23*, 235–242.
49. Domin, P.; Kovalenko, S.; Simkovic, F.; Semenov, S.V. Neutrino accompanied $\beta^\pm\beta^\pm$, β^+/EC and EC/EC processes within single state dominance hypothesis. *Nucl. Phys. A* **2005**, *753*, 337–363.
50. Raina, P.K.; Shukla, A.; Singh, S.; Rath, P.K.; Hirsch, J.G. The $0^+ \rightarrow 0^+$ positron double-β decay with emission of two neutrinos in the nuclei ^{96}Ru, ^{102}Pd, ^{106}Cd and ^{108}Cd. *Eur. Phys. J. A* **2006**, *28*, 27–36.
51. Suhonen, J. Double beta decays of ^{106}Cd. *AIP Conf. Proc.* **2011**, *1417*, 115–119.
52. Pirinen, P.; Suhonen, J. Systematic approach to β and $2\nu\beta\beta$ decays of mass A = 100 – 136 nuclei. *Phys. Rev. C* **2015**, *91*, 054309.
53. Ejiri, H. Fermi surface quasi particle model nuclear matrix elements for two neutrino double beta decays. *J. Phys. G* **2017**, *44*, 115201. [CrossRef]
54. Leoncini, A.; Belli, P.; Bernabei, R.; Cappella, F.; Caracciolo, V.; Cerulli, R.; Danevich, F.A.; Inchicchitti, A.; Kasperovych, D.V.; Klavdiienko, V.R.; et al. New results on search for 2β decay processes in ^{106}Cd using $^{106}CdWO_4$ scintillator. *Phys. Scr.* **2022**, *97*, 064006. [CrossRef]
55. Suhonen, J.; Aunola, M. Systematic study of neutrinoless double beta decay to excited 0^+ states. *Nucl. Phys. A* **2003**, *723*, 271–288. [CrossRef]

56. Rath, P.K.; Chandra, R.; Chaturvedi, K.; Raina, P.K.; Hirsch, J.G. Deformation effects and neutrinoless positron $\beta\beta$ decay of ^{96}Ru, ^{102}Pd, ^{106}Cd, ^{124}Xe, ^{130}Ba, and ^{156}Dy isotopes within a mechanism involving Majorana neutrino mass. *Phys. Rev. C* **2009**, *80*, 044303. [CrossRef]
57. Suhonen, J. Physics of Nuclear Processes Triggered by the Interplay of Strong and Weak Interactions. *J. Phys. Conf. Ser.* **2012**, *338*, 012030. [CrossRef]
58. Suhonen, J. Particle-, nuclear- and atomic-physics aspects of rare weak decays of nuclei. *Phys. Scripta T* **2012**, *150*, 014039. [CrossRef]
59. Rath, P.K.; Chandra, R.; Chaturvedi, K.; Lohani, P.; Raina, P.K.; Hirsch, J.G. Uncertainties in nuclear transition matrix elements for $\beta^+\beta^+$ and $\epsilon\beta^+$ modes of neutrinoless positron double-β decay within the projected Hartree-Fock-Bogoliubov model. *Phys. Rev. C* **2013**, *87*, 014301. [CrossRef]
60. Barea, J.; Kotila, J.; Iachello, F. Neutrinoless double-positron decay and positron-emitting electron capture in the interacting boson model. *Phys. Rev. C* **2013**, *87*, 057301. [CrossRef]
61. Staudt, A.; Muto, K.; Klapdor-Kleingrothaus, H.V. Nuclear matrix elements for double positron emission. *Phys. Lett. B* **1991**, *268*, 312–316. [CrossRef]
62. Belli, P.; Bernabei, R.; Brudanin, V.B.; Cappella, F.; Caracciolo, V.; Cerulli, R.; Danevich, F.A.; Incicchitti, A.; Kasperovych, D.V.; Klavdiienko, V.R.; et al. Search for Double Beta Decay of ^{106}Cd with an Enriched $^{106}CdWO_4$ Crystal Scintillator in Coincidence with $CdWO_4$ Scintillation Counters. *Universe* **2020**, *6*, 182. [CrossRef]
63. Rukhadze, N.I.; Gusev, K.N.; Klimenko, A.A.; Rozov, S.V.; Rukhadze, E.; Salamatin, A.V.; Simkovic, F.; Shitov, Y.A.; Stekl, I.; Timkin, V.V.; et al. New results for double beta decay of ^{106}Cd. In Proceedings of the Book of Abstracts of the LXXII International Conference NUCLEUS-2022, Moscow, Russia, 11–16 July 2022; p. 261.
64. Belli, P.; Bernabei, R.; Brudanin, V.B.; Cappella, F.; Caracciolo, V.; Cerulli, V.; Chernyak, D.M.; Danevich, F.A.; D'Angelo, S.; Di Marco, A.; et al. Search for decay of ^{106}Cd with an enriched $^{106}CdWO_4$ crystal scintillator in coincidence with four HPGe detectors. *Phys. Rev. C* **2016**, *93*, 045502.
65. Suhonen, J. Interplay of particle, nuclear and atomic physics in rare weak decays. *AIP Conf. Proc.* **2010**, *1304*, 85–93.
66. Belli, P.; Bernabei, R.; Boiko, R.S.; Brudanin, V.B.; Cappella, F.; Caracciolo, V.; Cerulli, R.; Chernyak, D.M.; Danevich, F.A.; D'Angelo, S.; et al. First Results of the Experiment to Search for 2β Decay of ^{106}Cd with the Help of $^{106}CdWO_4$ Crystal Scintillators. *AIP Conf. Proc.* **2010**, *1304*, 354–358.

Disclaimer/Publisher's Note: The statements, opinions and data contained in all publications are solely those of the individual author(s) and contributor(s) and not of MDPI and/or the editor(s). MDPI and/or the editor(s) disclaim responsibility for any injury to people or property resulting from any ideas, methods, instructions or products referred to in the content.